Galindo, J.; Climent, H.; De La Morena, J.; Pitarch-Berná, R.; Guilain, S.; Besançon, T. (2021). A methodology to study the interaction between variable valve actuation and exhaust gas recirculation systems for spark-ignition engines from combustion perspective. Energy Conversion and Management. 250:1-17. https://doi.org/10.1016/j.enconman.2021.114859

A methodology to study the interaction between variable valve actuation and exhaust gas recirculation systems for spark-ignition engines from combustion perspective.

José Galindo[a], Héctor Climent[a], Joaquín De la Morena[a,*], Rafael Pitarch[a], Stéphane Guilain[b], Thomas Besançon[b]

[a] *CMT-Motores Térmicos, Universitat Politècnica de València, Camino de Vera s/n, 46022 Valencia (Spain)*
[b] *Renault Nissan Mitsubishi, 1 Allée Cornuel Lardy 91510 (France)*

Abstract

Several technologies are being put in place to improve the efficiency of spark-ignition engines. Two of these technologies are variable valve actuation and exhaust gas recirculation, both of which can have an impact on combustion according to the literature. However, this impact is due to variations in both the in-cylinder temperature and composition, linked to the different characteristics of internal and external residuals, which are difficult to decouple. In this paper, a methodology aimed at improving the understanding of the temperature and composition effects on combustion parameters is developed. Internal residuals are controlled through a variable valve timing actuation, and evaluated thanks to a previously validated one-dimensional engine model, while the externally-circulated exhaust are extracted after the catalyst through a low-pressure system. Combustion is analyzed based on in-cylinder pressure acquisition and emissions measurement at the engine-out, before the aftertreatment module. Different combinations of internal and external residuals are tested with different strategies from the point of view of the spark actuation: first, a constant spark timing for each value of total residuals; then, a spark timing adapted to maintain the same temperature inside the cylinder at the combustion start, and

*joadela@mot.upv.es

final an optimized calibration from the point of view of the engine efficiency. Results show a general trend to enhance combustion timings as higher share of internal residuals are introduced for the same amount of total residuals. It can be seen how this trend comes mostly from the temperature effect at low total residuals fraction, while composition effects are more significant as the amount of total residuals increase. Empirical correlations developed in the paper confirm the need to decouple internal and external residuals to have a proper estimation of the combustion timings. Despite the positive impact of internal residuals on the combustion duration, a small fuel consumption benefit is reached with cooled exhaust gas recirculation thanks to lower heat transfer losses. In terms of emissions, unburned hydrocarbon emissions tend to be reduced with increasing the share of internal residuals thanks to the higher combustion speed, while other gaseous emissions are mostly affected by the total residuals amount. Therefore, internal and external residuals could be combined to achieve the best tradeoff between fuel consumption and hydrocarbon emissions.

Keywords:

Spark-ignition, EGR, residuals, combustion, emissions.

---

1. Introduction

The increasing awareness of people about the need to address the problem of greenhouse gases emissions and pollution in urban areas has led to more stringent emission regulations over the last few decades [1]. In this sense, new technologies have been implemented on spark-ignition engines in recent years. Joshi [2] highlights the synergies on fuel consumption of several technologies such as exhaust gas recirculation (EGR), variable valve actuation (including Miller cycle), variable compression ratio, turbocharging and lean combustion. Other techniques as pre-chamber injection, hybridization, electrification and fuels are also assessed. In terms of emissions, the well-stablished TWC (Three-Way Catalyst) is more and more complemented with a GPF (Gasoline Particle Filter) due to elevated PN (Particle Number) emissions. Different strategies as

pre-turbo catalysts and strategies focused on lean operation are also mentioned.

Variable valve actuation (VVA) can be used to reduce the need for throttling the engine at low-to-mid loads, reducing pumping losses and fuel consumption [3]. This is achieved through an increase of the residual gas fraction inside the cylinders during the intake stroke, which can affect combustion. Szwaja et al. [4] studied the effects of exhaust residuals on a natural gas fueled engine. NO_x (nitrogen oxides) emissions were notably decreased with higher residual concentrations. However, HC (hydrocarbons) and CO (carbon monoxides) were increased. On the combustion side, both the induction time (defined as the time elapsed between the spark activation and the 10% of the total heat released) and the combustion duration (calculated as the difference between the 10 and 90 percent of the heat released, i.e. CA10-90) were deteriorated, being the induction time much more sensitive to residuals concentration due to the higher importance of laminar flame speed in this portion of the combustion process. Lanzanova et al. [5] used negative valve overlap to achieve high internal residuals amount on a spark-ignition engine fueled with ethanol, providing advantages in pumping losses and combustion phasing at low engine speed (1500 rpm) and load (3 bar indicated mean effective pressure) conditions. Khoa et al. [6] investigated different strategies to control residual gas fraction under a wide range of speed and load conditions, varying also other control parameters, on a small motorcycle engine. Their study shows that the combination of early intake valve opening and late exhaust valve closing is the optimal way to control the internal residuals amount, and confirmed a positive impact in the reduction of combustion temperature and NO_x emissions. Malaquias et al. [7] studied the effects of running with high amount of internal residuals combined with different compression ratios and tumble motion in a single-cylinder flex-fuel direct injection engine. Results showed reduced pumping losses and a 2% increase in efficiency when operating with high internal residuals. This result may be explained by the use of early intake valve opening to increase the concentration of internal residuals. Besides, a slowdown on combustion time (CA10-CA90) is observed. In terms of emissions, the main pollutants were all reduced between

30 and 40 percent.

A more flexible way to increase the total amount of residuals trapped at the valves closure consists of using an exhaust gas recirculation (EGR) system. Apart from the fuel consumption improvement at low loads thanks to lower pumping losses, such systems have shown to reduce the need to enrich at high loads [8] to protect turbine components, reducing fuel consumption and emissions of hydrocarbons and carbon monoxides [9, 10]. Besides, EGR can help to reduce the knock tendency [11, 12], which can be translated into an efficiency increase [13] thanks to a better combustion phasing [14] or a compression ratio increase [15]. However, it has to be considered that a negative effect in laminar flame speed and combustion duration is induced by EGR, which can actually overcome the specific heat ratio and heat transfer benefits for some engine conditions, resulting in an indicated efficiency deterioration [16]. Yu et al. [17] studied the effects of EGR on emissions and combustion of an SI engine fuelled with gasoline and ethanol. The results showed a reduced induction time and time of combustion by increasing the ratio of ethanol injected even with EGR. Oh et al. [18] demonstrated the benefits and synergy of high tumble motion, EGR, Miller cycle and an electric supercharger in a hybrid electric vehicle. A 10% efficiency improvement was achieved in total and the maximum deployment increased by 23% at 2000 rpm, improving the dynamic response and performance. Gong et al. [19] compared the traditional EGR strategy with an only CO_2 EGR strategy. The results showed that only CO_2 EGR could reduce the variations on the IMEP (Indicated Mean Effective Pressure) compared to traditional EGR, as well as the CO, HC and soot emissions. The main advantage of traditional EGR was seen in NO_x reduction.

Different design alternatives can be found in the literature for the EGR circuit, affecting combustion and emissions due to differences in temperature and composition of the exhaust gases. Galloni et al. [20] and Yu et al. [21] analyzed the potential benefits from a cooled high-pressure exhaust gas recirculation (HP-EGR) system, characterized by the use of uncatalyzed exhaust gases, confirming the capability of the system to reduce enrichment and knock tendency at full-

load conditions, while a reduction in the maximum power capability. Xie et al. [22] compared the dilution effects with cooled and hot HP-EGR, resulting in a reduced ignition delay and combustion duration with hot EGR compared to cooled EGR, obtaining a better combustion phasing and reduced cycle-by-cycle variations.

Lujan et al. [23] studied instead a low-pressure exhaust gas recirculation (LP-EGR) system, where the exhaust gases are extracted after the catalyst. At partial loads, fuel consumption is reduced mainly due to a better combustion phasing and pumping losses reduction, being the reduction in heat losses a secondary factor. As expected, lower combustion temperatures led to reduced engine-out NO_x and increased HC emissions, which were also affected by longer combustion. At high loads, the fuel consumption reduction is greater than at low loads due to the fuel enrichment suppression, a better combustion phasing and reduced heat losses. On emissions side, NO_x is again decreased and HC increased. Major problems found on the study at high loads were: the increase of pumping losses and the need to re-match the turbocharger to achieve the same load, as well as water condensation on the intercooler. Furthermore, Reihaini et al. [24] showed that the usage of LP-EGR implies the need for higher boost pressure increasing the pumping work, which could be further affected by a loss of homogeneity of the flow field upstream the compressor depending on how the LP-EGR inlet is designed. Bermudez et al [25] analyzed in further details the impact of cooled LP-EGR on the catalyst performance, concluding that conversion efficiencies were reduced for HC and CO due to the lower oxygen content and temperature in the exhaust gases, while NO_x conversion efficiency was only compromised at high loads due to a reduction of raw CO emission. Franken et al. [26] combined single-cylinder engine experiments and tabulated chemistry simulations to analyze the effects of cooled LP-EGR and water injection on engine efficiency and raw emissions, confirming the capability of both systems to reduce knock and increase indicated efficiency, while a negative impact of LP-EGR on soot formation was identified. Lattimore et al. [27] analyzed in further details the impact of EGR on soot emissions. At high

load, the reduction of enrichment achieved with EGR provides an advantage in particles formation. Instead, at lower loads the soot emissions trend is directly affected by the ignition timing: if similar combustion phasing in terms of CA50 is controlled, longer combustion duration induced by moderate EGR rates results in the oxidation of the accumulation mode particles at the latests stages of combustion, thus reducing the soot particle emissions [28]. Instead, if the EGR level is increased the negative effect of the reduced combustion temperature over the soot particles oxidation is dominant, and an increase in the soot emissions is achieved. Zhao et al. [29] used hydrogen enrichment in the EGR gases as well as isobutanol-gasoline blends as means to overcome the negative effect of EGR on combustion duration and stability, reaching positive results both from thermal efficiency and exhaust emissions perspective. Gainey et al. [30] also showed that alcohol-based fuels can help to improve EGR tolerance.

Despite the aforementioned studies show that both VVT and EGR can be identified as technologies capable to control the residual gas fraction inside the cylinder and achieve thermal efficiency improvements, few works have analyzed in detail the relative impact of both systems. Galindo et al. [31] combined experimental engine data with 1-dimensional simulations to study the interaction between VVT and LP-EGR in terms of internal residuals trapping, pumping losses and indicated efficiency. Their results show that VVT settings play a significant role in the internal residuals trapped for low load operation, implying a more significant interaction with the external EGR. Instead, as the load increases the main effect of VVT is related to the pumping work as a consequence of the interaction with the variable geometry turbine available in the engine used for that study. However, the individual effects of internal residuals (controlled by the VVT) and cooled LP-EGR from combustion and emissions perspective were not investigated in detail. A proper differentiation of the individual effects of these two different dilution methods could be of interest for adapting phenomenological SI combustion models [32] which can predict combustion phasing trends, needed for 1-dimensional engine simulations, without the need for a detailed chemical kinetic model.

Considering all the information from the literature, the main objective for this study is to develop a methodology to investigate the individual effects of external exhaust gas recirculation (EGR) and internal residuals (IGR) on combustion performance. With that goal, an experimental campaign is carried out on a spray-guided spark-ignition engine with variable valve timing system at intake and exhaust camshafts, a variable geometry turbine and a cooled low-pressure EGR loop. The campaign focuses on the mid-to-low engine load, where as explained before the range of variation of the internal residuals is more significant. The experimental matrix includes three evenly spaced levels of total residual gas fraction (RGF). To decouple the effects of the composition and temperature of these residual gases, each RGF level is achieved by four different combinations of internal residuals (IGR) and cooled LP-EGR by a proper control of the VVT and EGR systems. IGR is estimated through a previously developed and validated one-dimensional engine model on GT-Power. Finally, three different spark actuation strategies are considered. Initially, a constant spark timing is selected for each RGF level. Then, the spark timing is adapted to achieve the same charge temperature at the spark activation point, so that the relative importance of this temperature on the combustion speed can be better identified. Finally, the spark is set to optimize the indicated efficiency, so that the comparison between internal and external residuals can be made on a more realistic condition from a system level perspective.

As far as the paper structure is concerned, the study is divided in five sections. Section 2 describes the experimental facility and instrumentation used for the study. Next, the methodology used to calibrate the engine settings (in terms of VVT, EGR and spark) for each experiment is described in Section 3. Section 4 focuses first on the comparison between constant-spark and constant-temperature conditions, based on laminar flame speed considerations, while the analysis of the optimized spark timing tests is performed in Section 5. Finally, the main conclusions drawn from the whole study are summarized in Section 6, while Section 7 discusses the limitations of the methodology and proposes some future works in the field.

2. Experimental set-up

A four-cylinder 1.3L spark ignited direct-injection engine is used for this study. The engine includes a variable geometry turbine (VGT) as well as a variable valve timing system (VVT), which is able to advance or delay the actuation of the intake and exhaust valves independently, maintaining the duration of the event. The range of variation of this VVT system runs from zero to forty crank angle degrees, corresponding to minimum and maximum overlap condition respectively (i.e. forty degrees would delay the exhaust and advance the intake). A prototype low-pressure (LP) EGR line is installed to the production engine. The line extracts the exhaust gases downstream the three way catalyst (TWC), and introduces them into a T-joint placed upstream the compressor. The exhaust gases are cooled down at a plate and fin cooler fed with engine coolant at approximately 90°C and routed by an EGR valve. Finally, an additional valve is placed upstream the T-joint to enlarge the amount of recirculated exhaust gas by inducing a greater pressure differential between intake and exhaust, particularly necessary for low speed and load conditions. Once mixed with the fresh air and pressurized in the compressor, a second cooling is achieved in a water charge-air cooler (WCAC) integrated in the intake manifold, targeted to reduce the charge temperature up to approximately 30°C. The main characteristics of the engine are summarized in Table 1.

Table 1: Engine main characteristics.

Magnitude	**Units**	**Value**
Engine type	[-]	4-stroke turbocharged
Number of cylinders	[-]	4
EGR circuit	[-]	Cooled low-pressure
Turbocharger	[-]	VGT
Displaced volume	[cc]	1300
Stroke	[mm]	81.2
Bore	[mm]	72
Compression ratio	[-]	10.6:1

The engine is mounted on a test bench with a dynamometric brake AVL AFA 200/4-8EU, handled by an AVL-PUMA software to allow for speed and torque control. A partially opened ECU is installed so that VVT, spark advance and throttle valve position could be modified for the tests. All the variables coming from the ECU are saved through INCA v7.1.

In order to control the VGT and EGR valves, an open loop configuration based on a National Instruments PXI system, as described in [33], is used. This system is also useful to record high-frequency data. This includes the instantaneous pressure in all cylinders, acquired through instrumented spark-plugs (AVL ZI33), and the pressure at intake and exhaust manifolds (by means of Kistler 4007 piezorresistive sensors). Additionally, online calculations such as the indicated mean effective pressure (IMEP) and its coefficient of variation (COV), the apparent heat release rate and knock estimation by the maximum amplitude of the pressure oscillations (MAPO) are computed.

The instrumentation of the engine also consists of type K thermocouples and mean pressure sensors along the intake, exhaust and EGR lines. An AVL FlowsoniX Air flowmeter and an AVL 733S gravimetric balance are used to obtain air and fuel mass flows, respectively. Turbocharger speed is measured by a MICRO-EPSILON DS05 sensor. A HORIBA MEXA-ONE is connected

to provide raw emissions upstream the TWC, with another connection at the intake line to estimate the EGR rate [34, 35] as shown in Equation 1:

$$EGR_{rate} = \frac{[CO_{2,int}] - [CO_{2,atm}]}{[CO_{2,exh}] - [CO_{2,atm}]} \cdot 100 \quad (1)$$

where $[CO_{2,int}]$, $[CO_{2,exh}]$ and $[CO_{2,atm}]$ are the molar fraction as Vol.% of CO_2 at intake, exhaust and ambient respectively. A summary of the sensors used, their measuring uncertainty and range can be found in Appendix A.

A diagram of the engine set-up is shown below in Figure 1. A summary of all the sensors used, their measuring uncertainty and range can be found in appendix A.

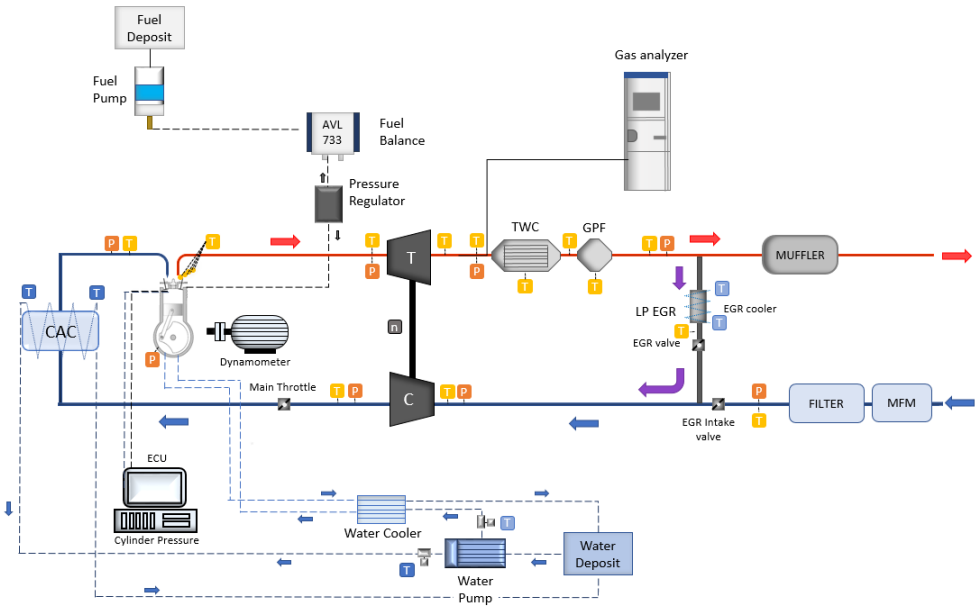

Figure 1: Engine set-up diagram.

The fuel used in this study is a 98 Research Octane Number (RON) commercial gasoline, which main properties are shown in Table 2.

Table 2: Fuel main properties.

Magnitude	**Units**	**Value**
Fuel	[-]	Gasoline
RON	[-]	98
Carbon content	[%]	85.98
Hydrogen content	[%]	12.09
Nitrogen content	[%]	<0.01
Sulfur content	[mg/kg]	7.83
Upper heating value	[MJ/kg]	45.31
Lower heating value	[MJ/kg]	42.82

3. Methodology

As expressed in the introduction, the main purpose of the study is to define a methodology to evaluate the individual effects of internal residuals and external EGR on the combustion process of a spark-ignition engine. For that purpose, the experimental campaign aims to cover different levels of total residual gas fraction (RGF), each of them achieved by different combinations of internal residuals and external EGR. First, the operating conditions most suitable to achieve a high magnitude of total residuals combined with a high range of variation of their composition will be selected; then, the methodology used to analyze the temperature and composition effects of these residuals will be described. In this sense, several engine operating conditions are considered at first in the search of a high variation of internal residuals with the VVT system. Finally, a model validation section including the results from the selected conditions will be discussed.

3.1. Selection of engine operating point

While external EGR can be obtained in the test bench according to Equation 1, there is not a direct measurement of the internal residuals nor the total

residual gas fraction. Therefore, a procedure to estimate these quantities needs to be put in place.

In particular, a previously developed and validated one-dimensional engine model built in GT-Power [31, 36] is used. In a first step, this model allows to evaluate the internal residuals in a set of experimental data from a Design of Experiments (DoE) previously performed in the same engine at different engine speed and loads. In particular, the DoE covers 50 different combinations of spark advance, intake and exhaust VVT and EGR rate for each engine speed and load. More details about the DoE construction and postprocessing can be found in [34].

The GT-Power model reproduces the experimental information with the following strategy:

- The intake and exhaust valve timings are set according to the values controlled through the ECU.
- The experimental EGR rate is achieved by the positions of the EGR and intake valves of the LP-EGR circuit.
- Compressor and turbine are decoupled, so that the compressor outlet pressure (P2) and the exhaust manifold pressure (P3) can be set independently. Additionally, the main engine throttle controls the intake manifold pressure (P2'). In this way, the pressure boundary conditions across the engine, which determine the engine trapping ratio together with the characteristics of the valve events, are matched.
- The intake manifold temperature defines the heat transfer characteristics in the WCAC, and the air mass flow is refined through the adaptation of the overall heat transfer multiplier in the cylinders.
- Fuel mass flow is set according to the experimental lambda measurement, while the combustion is reproduced by a Wiebe function, which is using the experimental values of combustion start, crank angle for the 50% of total heat released (CA50) and total combustion duration (defined in terms of

10 to 90% of the total heat released) obtained from the in-cylinder pressure analysis from a total of 800 cycles (200 cycles acquired for each of the 4 engine cylinders). The heat release rate used to compute these combustion timings was extracted using an in-house zero-dimensional one-zone combustion diagnostic model called CALMEC, including heat transfer losses and mechanical deformations according to a previous characterization of the engine from motoring test data according to the procedure described in Payri et al. [37].

The minimum (blue) and maximum (orange) IGR concentration obtained with the 1D model for each operating condition tested is shown in Figure 2.

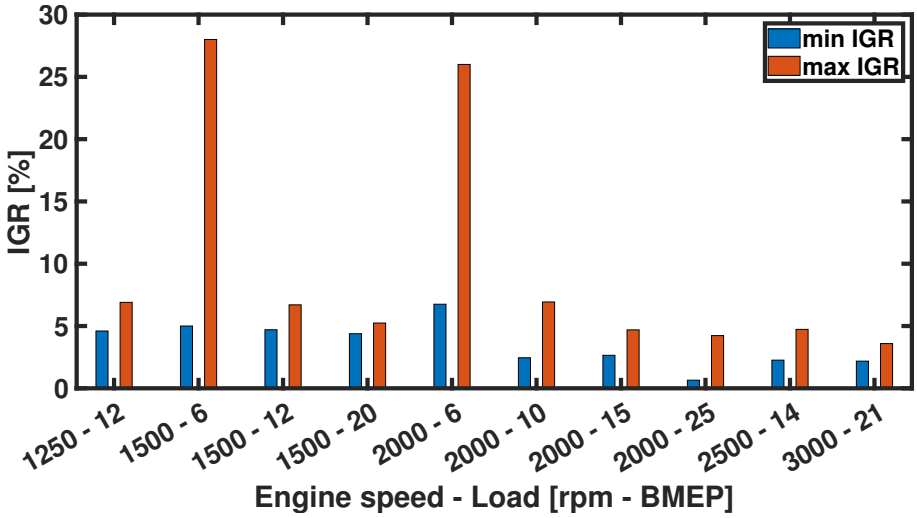

Figure 2: Minimum (blue) and maximum (orange) IGR concentrations obtained at several engine speed and load conditions based on 50 experimental tests DoE.

As it can be seen, for most of the points the range of variation of the internal residuals is very limited. One the one hand, engine loads in the range of 12 bar BMEP or higher imply boosted operation, for which the difference between intake and exhaust manifold pressures is smaller compared to lower loads, where the intake manifold is throttled. Additionally, the suitable operation of the VVT system at low speeds and higher loads is restricted by scavenging process, which

can affect fuel control by the ECU. With all this in mind, a low speed and load condition (in particular, 1500 rpm and 6 bar BMEP) has been selected for the analysis, since the range of variation of the internal residuals is the highest, and therefore the impact on combustion can be more significant.

3.2. Experimental conditions for selected operating point

Once the most suitable speed and load condition is identified, data is screened looking for three equally spaced RGF rates: 13%, 20% and 27%. For each of these rates, the objective is to find the combinations of VVT and EGR that would give different distributions of the amount of EGR and IGR with respect to the total RGF. In particular, points as close as possible to the ones highlighted in Table 3 distributions are targeted:

Table 3: EGR and IGR distributions sought for each RGF rate.

Point	**% EGR in RGF**	**% IGR in RGF**
1	75	25
2	50	50
3	25	75
4	0	100

As it could be expected, the combination of 100% EGR in RGF is unreachable, since some internal residuals are always present, especially at low loads. Besides, when there is no test that meets a specific distribution, a new simulation in GT-Power is run to find the combination of VVT at a given EGR that would achieve the desired IGR. For that purpose, since there is not an experimental measurement, the 1D model is adapted to operate in predictive mode. Therefore, turbine and compressor are reconnected, and the rest of the model parameters are set based on empirical correlations built from the data obtained in the aforementioned DoE. Once the VVT and EGR combination that provides the targeted IGR and RGF levels is found by the model, it is tested in the

engine and the data is reprocessed in the 1D engine model using the methodology previously described, in order to ensure that the intended composition was reached.

Following these steps, the experimental points shown in Table 4 will be used for the study. The table details the total RGF level, intake and exhaust VVT settings, EGR and IGR. Additionally, EGR and IGR are displayed not only as an absolute value but also as a percentage with respect to the total amount of residuals in brackets.

Table 4: Main parameters of the engine tests.

RGF [%]	**Point** [–]	**Int - Exh VVT** [°]	**EGR [% in RGF]** [%]	**IGR [% in RGF]** [%]
13	1	1 - 0	9 [65]	5 [35]
	2	9 - 10	6 [47]	7 [53]
	3	20 - 10	3 [25]	9 [75]
	4	0 - 35	0 [0]	13 [100]
20	1	18 - 9	15 [71]	6 [29]
	2	15 - 21	10 [53]	9 [47]
	3	16 - 33	5 [25]	15 [75]
	4	24 - 29	0 [0]	19 [100]
27	1	30 - 2	22 [78]	6 [22]
	2	24 - 32	13 [48]	14 [52]
	3	37 - 33	5 [20]	20 [80]
	4	37 - 33	0 [0]	23 [100]

Once the VVT and EGR levels or interest are defined, and provided that the engine runs in stoichiometric conditions, there is still an important open point in the engine control that will affect the combustion assessment: the spark actuation. If a constant spark timing is set, two contributions are expected when comparing EGR vs. IGR at the same total residuals level: on the one hand, a higher amount of internal residuals implies a warmer temperature at the intake

valve closure (IVC) and therefore at the spark activation time, inducing higher laminar flame speed; on the other hand, since a low-pressure EGR circuit is used, the gases recirculated externally are passed through the TWC, affecting their composition, which can have some impact on combustion development. Taking all these aspects into account, three different calibration strategies are evaluated:

1. **Isospark**: All points in each RGF group are tested with the same spark advance, set to minimize combustion instability (in terms of the covariance of the IMEP) for the tests with the minimum amount of internal residuals (i.e. minimum valve overlap).
2. **Isotemperature**: In order to decouple the aforementioned temperature and composition effects, a new test adjusting the spark for each IGR-EGR combination is targeted to reach the same temperature at the spark timing. For that purpose, experimental data are obtained first with a late spark activation and processed in the 1D engine model, so that the temperature across the whole compression stroke can be evaluated without any combustion impact. Then, the crank angle at which a certain temperature value is reached can be identified for each IGR-EGR case. In particular, 760 K at the spark event is selected.
3. **Optimal spark**: Spark timing is adapted so that the indicated efficiency is maximized. This results in a combustion phasing characterized with a CA50 between 7 and 9 CAD, consistent with previous works in the literature [38].

Table 5 shows the resulting spark advances used for the aforementioned spark actuation strategies. As it can be seen, as the RGF increases the spark needs to be advanced with respect to TDC to optimize combustion stability in the isospark tests. Instead, for the isotemperature tests, more advanced sparks are observed as both the total RGF and the IGR levels increase in order to compensate for the higher initial in-cylinder temperature, as it could be expected. Regarding the optimal spark, actuations are around 5 crank angle

Table 5: Spark advance settings for each calibration strategy.

RGF	**IGR**	**Spark Advance**		
	Value [% in RGF]	**Isospark**	**Isotemperature**	**Optimal**
[%]	[%]	[°bTDC]	[°bTDC]	[°bTDC]
13	5 [35]	6	9	11
	7 [53]	6	14	11
	9 [75]	6	18	10
	13 [100]	6	17	11
20	6 [29]	10	15	16
	9 [47]	10	18	15
	15 [75]	10	20	14
	19 [100]	10	22	13
27	6 [22]	15	17	21
	14 [52]	15	20.5	19.5
	20 [80]	15	24.5	19
	23 [100]	15	24.2	17

degrees (CAD) more advanced than the isospark tests, showing that it is advantageous to center the combustion in the initial stages of the expansion stroke despite a slight deterioration in combustion stability is reached. Comparing different IGR values, the spark activation is practically equal for all cases when the total amount of trapped residuals is low (13%), while for higher RGF levels there is a slight trend to delay the spark activation as the IGR increases. This can be seen as a first indication of a positive effect of IGR in combustion speed, since the CA50 is approximately constant, so a later spark actuation implies a shorter duration of the first phase of the combustion event.

Once the tests were completed, they were simulated again on GT-Power, giving a maximum deviation of 0.5% in the absolute value of the internal residuals between the different spark calibration strategies. Figure 3 shows the temper-

ature at the spark event comparing the isospark and isotemperature cases. In this chart, the color and symbol describe the residual gas fraction level (orange circles: 13%; blue diamonds: 20%; green squares: 27%), while the line style differentiates the calibration strategy (solid line: isospark; dashed line: isotemperature). As it can be seen, isotemperature analysis demonstrates that the targeted temperature was reached with a variation between cases below 10 K. Instead, the isospark values are generally characterized by an increasing temperature as the IGR is higher, while the variation between different RGF levels is less significant due to the fact that higher amounts of residual gas fraction imply higher temperature at the cycle start but this effect is compensated by the more advanced spark timing.

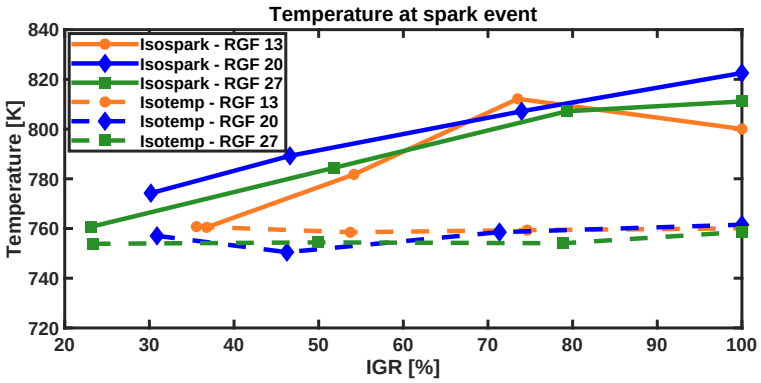

Figure 3: Temperature at spark event comparison between Isospark and Isotemperature tests with respect to IGR.

In order to keep constant the operating conditions of 1500 rpm and 6 bar BMEP for each test, the main engine throttle was adjusted individually. This was necessary due to the change in volumetric efficiency induced by the variations of VVT as well as the intake pressure due to the EGR rate. The main throttle values used are shown in Table 6. Besides, the injection was kept constant at 82 CAD after the start of the intake stroke .

Table 6: Main throttle settings for each calibration strategy.

RGF	**IGR**	**Main Engine Throttle**		
	Value [% in RGF]	**Isospark**	**Isotemperature**	**Optimal**
[%]	[%]	[°]	[°]	[°]
13	5 [35]	12.2	12.3	12.2
	7 [53]	11.8	11.8	11.8
	9 [75]	11.6	11.8	11.6
	13 [100]	11.2	11.7	11.1
20	6 [29]	13.3	13.2	13.0
	9 [47]	12.5	12.8	12.5
	15 [75]	12.1	12.7	12.0
	19 [100]	11.4	12.1	11.4
27	6 [22]	14.9	14.8	14.4
	14 [52]	13.8	14.0	13.7
	20 [80]	13.6	14.2	13.6
	23 [100]	12.8	13.6	12.8

3.3. Model validation

In this section, a brief explanation of the model validation process is carried out. This validation process has been used for all simulations made with the model. However, the description will be based on the final tests used for this study, depicted in Table 4 and for the optimal spark setting.

All final tests in this study were reproduced with the model in its fitting configuration, so intake and exhaust pressures were imposed, as aforexplained. In this sense, the remaining parameters that can most affect the concentration of residuals and that therefore the model must reproduce well are the air mass flow and the pressure pulses in the manifolds. Given the low engine load, a maximum error of a 10% in air mass flow with respect to the experimental value is set. The air mass flow, intake and exhaust pressure errors with respect to the experimental values is shown in Figure 4. Note that the x-axis represents a case number that corresponds from point 1-13% RGF to point 4-27% RGF in Table 4 and the optimal spark setting.

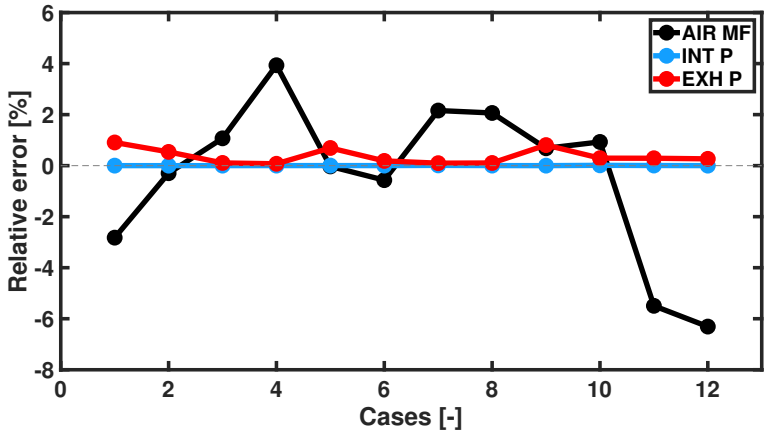

Figure 4: Air mass flow (black), intake (blue) and exhaust pressure (red) errors with respect to experimental values .

The instantaneous intake and exhaust pressures with respect to the crank angle degree are compared to the model. With this aim, two very different VVT

settings, point 2-13% RGF and point 4-27% RGF (corresponding to cases 2 and 12 in the previous figure), are chosen and shown in Figure 5 and Figure 6.

4. Temperature and composition effects

Firstly, a comparison between isospark and isotemperature is performed in order to shed light to the individual effects of the different composition and temperature for the residuals distribution, as previously discussed.

Figure 7 shows a comparison of the induction time, defined as the difference between the spark activation and the crank angle for 10% of the total heat released (CA10). Again, solid lines represent isospark tests while dashed lines the isotemperature conditions, while symbol and color define the different levels of residual gas fraction as defined for Figure 3. For the Isospark tests, advancing spark with higher RGF levels is translated into more advanced CA10 for both RGF levels. This can be partially understood considering the effect that temperature has on the laminar flame propagation speed:

$$S_L(\phi, T_u, P_u) = S_{L0} \left(\frac{T_u}{T_0}\right)^{\alpha} \left(\frac{p_u}{p_0}\right)^{\beta} \tag{2}$$

where S_L is the laminar flame speed at a given condition, S_{L0} is the laminar flame speed at standard conditions ($T_0 = 298K$ and $p_0 = 0.1MPa$), T_u and p_u are the temperature and pressure conditions in the unburned zone, and α and β are the coefficients assessing the temperature and pressure dependency. It has to be considered that these two coefficients would depend on the unburned zone composition, including the kind of fuel, the equivalence ratio and the amount of residuals. For stoichiometric conditions without residuals and gasoline fuel values of 1.69 and -0.278 can be considered according to the literature [39]. Given the fact that isospark tests are characterized by approximately the same pressure conditions at the spark timing, the only expected effects when changing the IGR level would be the temperature and the residues . Considering the data reported in Figure 3, a maximum increase in the initial laminar flame speed of approximately 11% could be expected when increasing the amount of IGR for

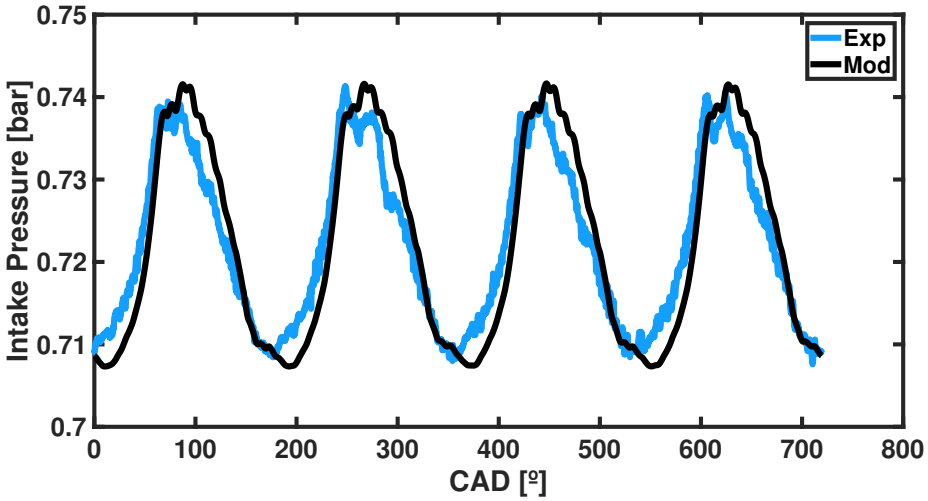

(a)

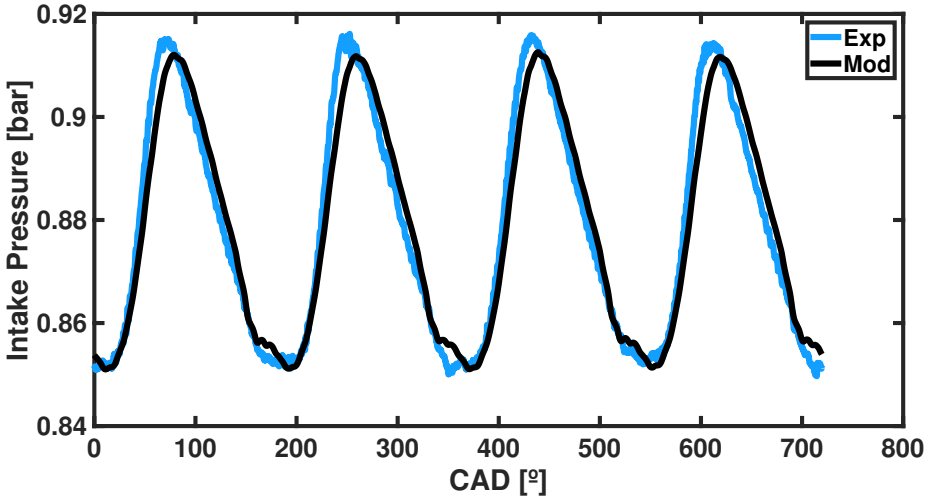

(b)

Figure 5: Intake pressure evolution with respect to crank angle degree comparison between experimental side (blue) and model (black) for point 2-13% RGF (a) and point 4-27% RGF (b).

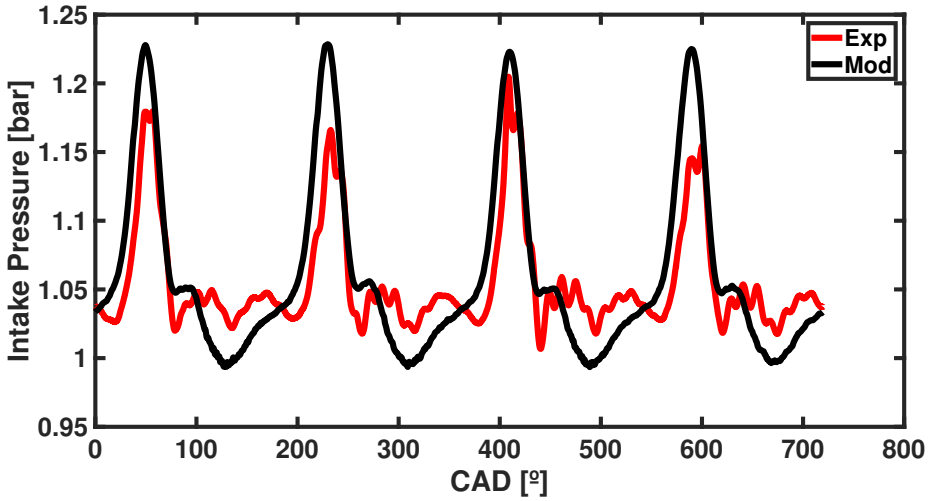

(a)

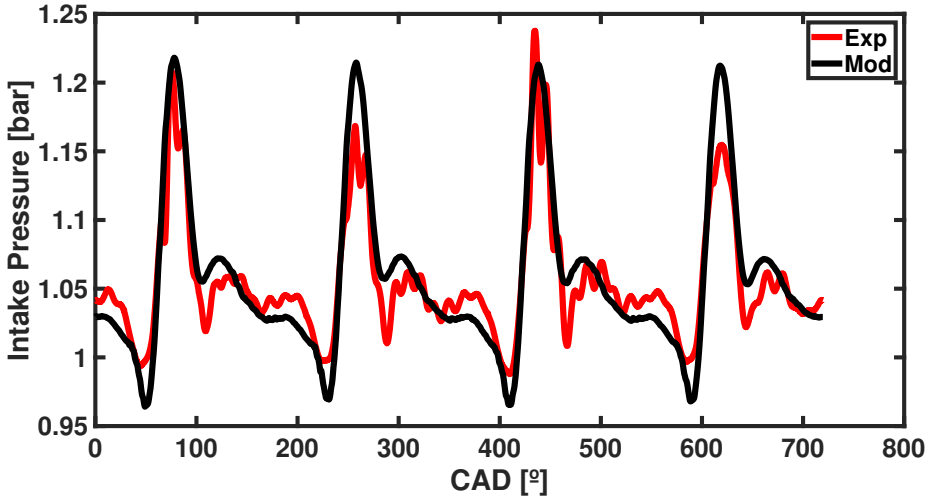

(b)

Figure 6: Intake pressure evolution with respect to crank angle degree comparison between experimental side (blue) and model (black) for point 2-13% RGF (a) and point 4-27% RGF (b).

both RGF levels, which would result in a decrease of the induction time of 1.5 CAD for the 13% RGF case, and 2.3 CAD for the 27% RGF condition. Comparing these values with the information depicted in Figure 7, the range of variation achieved in the induction time for the 13% could be fully explained by the temperature effect on the laminar flame speed. When comparing with the results from the isotemperature study, the induction time trend reverses, implying a deterioration when the IGR is higher, probably linked to changes in the local flow conditions around the spark plug [40, 41]. Instead, in the 27% the variation of induction time observed in the isospark tests (4 CAD) is clearly higher to the expectation from laminar flame speed analysis (2.3 CAD), indicating than in this case there is an effect from the different composition of the residual gases, since external EGR is characterized by a lower reactivity after passing through the TWC. Indeed, the isotemperature tests provide a lower induction sensitivity (3 CAD), closer to the expected effect from laminar flame speed considerations.

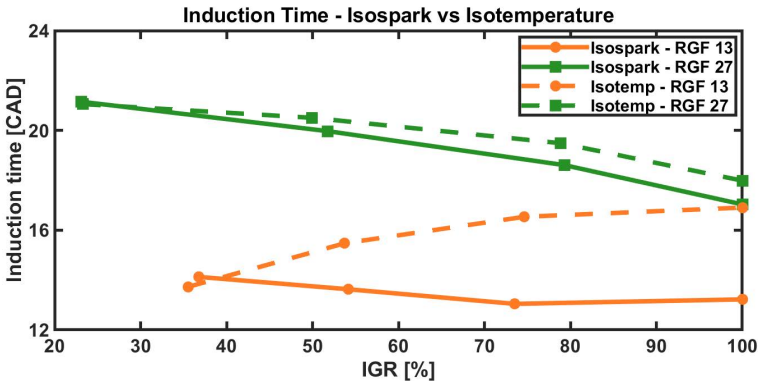

Figure 7: Induction time comparison between isospark and isotemperature tests with respect to IGR.

Figure 8 shows a similar comparison from the point of view of the time of combustion (TOC), computed as the difference between the 10 and 90 % of the heat released (CA10-90). In this case, both isospark and isotemperature tests for the 13 % RGF condition show almost no sensitivity of the combustion duration

with respect to the internal residuals amount, confirming that when the amount of residuals is low the impact of their composition is negligible. Instead, for the 27 % RGF a clear decreasing trend of the combustion duration with respect to the IGR level can be identified, regardless the testing strategy used. Another interesting aspect to highlight is that while at low IGR conditions (so when the total residuals are mostly achieved by cooled LP-EGR) there is a clear increase in the combustion duration when moving from 13 to 27 % of total RGF, as a consequence of the higher dilution, such effect is clearly diminished when the share of internal residuals is high. Therefore, some addition of internal residuals controlled through VVT could be seen as a way to reduce the negative impact of cooled LP-EGR on combustion performance.

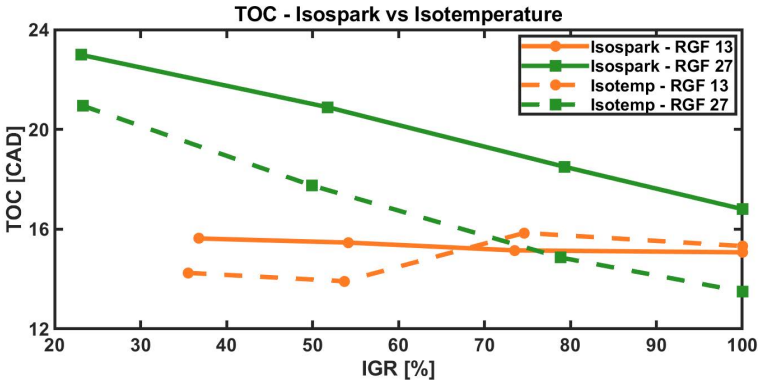

Figure 8: Time of combustion comparison between isospark and isotemperature tests with respect to IGR.

When the RGF rate is obtained entirely with IGR, a clear trend is obtained to increase the induction time for both conditions and a longer combustion for the isospark tests, as reported by Lanzanova et al [5]. Szwaja et al. [4] obtained the same trends, increasing the induction time and the time of combustion by 34 and 20% respectively with IGR.

The statistical variability of the combustion timings obtained from the in-cylinder pressure analysis are computed. The standard deviation of the induction time and TOC for the isospark and isotemperature tests is shown in Table 7.

Table 7: Standard deviation of the induction time and TOC for the isospark and isotemperature tests.

RGF	**IGR**	**Std Induction Time – Std TOC**	
	Value [% in RGF]	**Isospark**	**Isotemperature**
[%]	[%]	[°]	[°]
13	5 [35]	1.96 - 2.74	1.86 - 2.32
	7 [53]	1.83 - 3.08	1.43 - 1.47
	9 [75]	1.41 - 2.53	1.24 - 0.83
	13 [100]	1.84 - 2.97	1.20 - 0.83
20	6 [29]	2.17 - 4.42	1.26 - 2.79
	9 [47]	1.96 - 3.63	1.72 - 2.12
	15 [75]	1.92 - 3.42	1.24 - 0.95
	19 [100]	1.73 - 2.59	1.20 - 1.00
27	6 [22]	2.87 - 6.48	2.55 - 4.97
	14 [52]	2.44 - 5.09	2.20 - 3.35
	20 [80]	2.19 - 3.56	1.66 - 1.40
	23 [100]	2.19 - 3.02	1.59 - 1.06

Results show a reduction trend as the IGR increase, especially for high amounts of total residuals, owing to a higher temperature at the start of combustion and the increased presence of unburned components that would facilitate the development of the flame front.

The previous results have served to note that there is a direct impact of the different compositions of internal residuals and external EGR on the combustion performance. In this sense, empirical correlations are developed to better assess this effects on combustion. The empirical correlations can be seen in Appendix B. The results show that it is possible to predict the induction time as a function of RGF, IGR, spark timing (linked to turbulence effect) and the

thermodynamic conditions at the spark timing, while the capability of such correlations is severely impaired if only the total amount of RGF is considered.

5. Optimal Spark analysis

As stated during the description of the methodology (Section 3), the data presented up to know was achieved adjusting the spark activation timing to either minimize the combustion instability (isospark) or to achieve approximately 760K at combustion start (isotemperature). However, normally the spark is calibrated in these low speed and load operating area with the objective to maximize the engine thermal efficiency without overcoming a certain combustion instability threshold. The results extracted from such procedure are analyzed in this subsection. In particular, a limit of 3.3% in terms of the COV of the IMEP was set.

5.1. Combustion timings prediction

Figure 9 shows the data of the optimized calibration in terms of the induction time. Again, the color and symbol describe the residual gas fraction level (orange circles: 13%; blue diamonds: 20%; green squares: 27%). Additionally, solid lines show the experimental results, while the dashed lines refer to the values estimated from the empirical correlation previously achieved based on the isospark and isotemperature data. The graph shows the previously described trends for the induction time, increasing with the total amount of residuals but decreasing when a higher share of these residuals are trapped internally by the VVT system, as a consequence of the higher reactivity. These trends are properly captured by the empirical correlation, despite showing a slight overestimation in general except for the cases with the highest amount of cooled EGR (27% RGF with lowest levels of IGR).

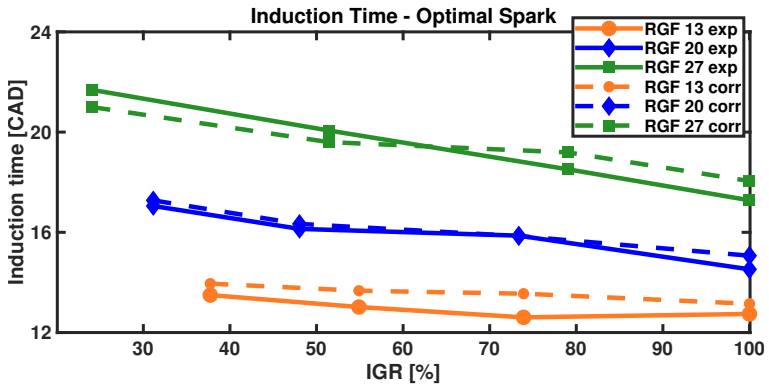

Figure 9: Induction time vs. IGR for optimal spark calibration.

Figure 10 depicts the combustion duration information using the same structure. Similar results as already seen for the induction time can be observed, with a maximum deviation between experimental and estimated values of the combustion duration of approximately 1 CAD. It shall be noted that since the TOC correlation proposed in the current work depends on the induction time, the estimated induction time values were used, so that the comparison of experimental vs. estimated TOC provides a valid assessment of the predictive capability of the correlations.

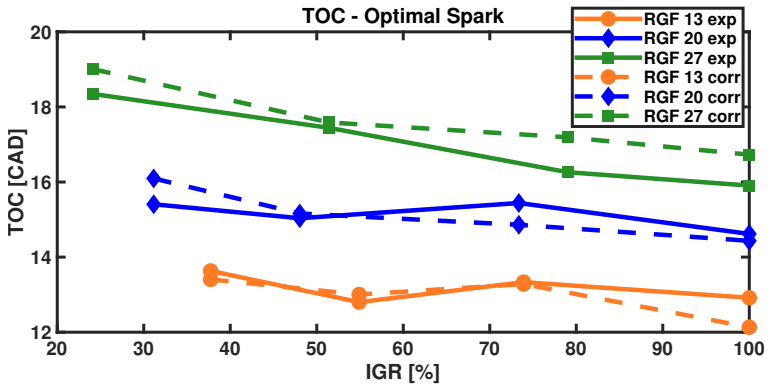

Figure 10: Combustion duration (TOC) vs. IGR for optimal spark calibration.

As already stated, the effect of increasing the IGR rate without EGR is directly linked to a slower combustion. This is observed both on the induction

Table 8: Standard deviation of the induction time and TOC for the optimal spark tests.

RGF	**IGR Value [% in RGF]**	**Std Induction Time**	**Std TOC**
[%]	[%]	[°]	[°]
13	5 [35]	1.73	1.91
	7 [53]	1.70	2.32
	9 [75]	1.48	2.16
	13 [100]	1.66	2.09
20	6 [29]	2.01	3.07
	9 [47]	1.85	2.58
	15 [75]	1.76	2.51
	19 [100]	1.68	2.29
27	6 [22]	2.27	3.80
	14 [52]	2.32	3.22
	20 [80]	2.21	2.75
	23 [100]	2.14	2.61

timing and the combustion duration, with a greater effect on the first as stated in [4]. This effect was also observed by Malaquias et al. [7], which studies reflected an increase of 5 CAD in the combustion duration when increasing IGR.

Again, the standard deviation of the induction time and TOC is shown in Table 8.

As in the isotemperature and isospark tests, results show a clear reduction of the deviation for both induction time and TOC as the IGR rate increases for a given RGF level. Naturally, as the RGF level increases, a slight increase in deviation is obtained.

5.2. Energy balance

Once the spark timing was optimized for each RGF and IGR level in order to maximize the engine thermal efficiency, it is possible to evaluate the impact of the VVT and EGR settings on the overall thermal balance, in order to provide further insights of the relative interaction of both systems. For this purpose, the heat transfer losses inside the cylinder and the enthalpy available in the exhaust gases have been computed from the one-dimensional engine model previously defined and validated. Heat transfer is computed based on an adapted Woschni model, for which the coefficients have been previously tuned based on motored engine tests at different speeds and throttle positions (i.e. intake pressure values). In this sense, values of 3.24 for the constant term (C1) and 1.91 for the tumble flow effect (C2) were attained.

This information is depicted in Figure 11. In this figure, the x-axis represents again the IGR level; the color specifies the total residual gas fraction level (orange: 13%; green: 27%); and the color intensity is used to distinguish the main three contributions from the fuel energy delivery: gross indicated efficiency (dark), which includes the complete 720 CAD cycle, heat transfer losses to the walls (intermediate) and enthalpy through the exhaust gases (light). As it can be seen, there is a trend to reduce the energy lost to the exhaust gases when increasing the amount of internal residuals, due to the shorter combustion duration that implies a reduction in the exhaust temperature, this is mostly compensated by an increase of the heat transfer losses during compression and combustion from the higher temperature at the intake valves closure. Therefore, the indicated efficiency remains approximately constant, with a slight decrease with the amount of internal EGR and some increase with the total amount of RGF.

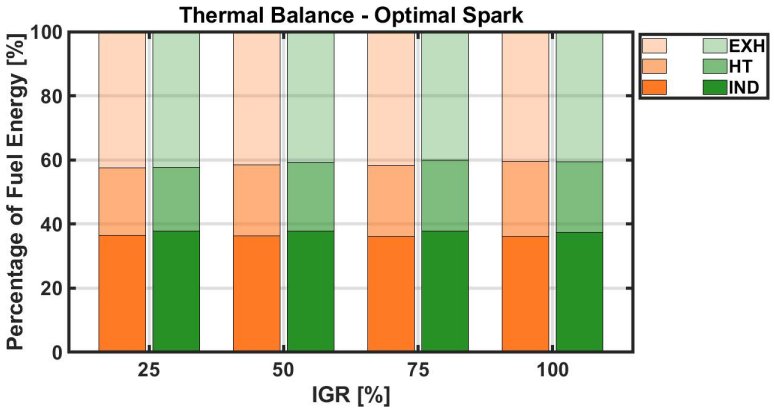

Figure 11: Thermal energy balance inside the cylinder as a function of IGR level for 13% (orange) and 27% (green) RGF level.

However, since the indicated efficiency computed considers the complete engine cycle, there is a portion of indicated work that is lost in the power transmission to the crankshaft as a combination of pumping and mechanical losses. Given the fact that the operating point and combustion phasing are approximately constant, few differences are found from friction losses perspective, so the main impact between different IGR levels are found on the pumping work. This information is provided in Figure 12 as a percentage variation with respect to the 27% RGF level achieved with only internal residuals, which is used as datum. The results show a general trend to reduce pumping work as the RGF increases, while the IGR impact is only clear for the 27% RGF sweep. For operation without EGR, reduced pumping losses are obtained as the RGF rate increases due to a higher portion of IGR. These results agree with those obtained by Malaquias et al. [7], who reported a reduction in pumping losses between 14 and 10% as residuals are increased.

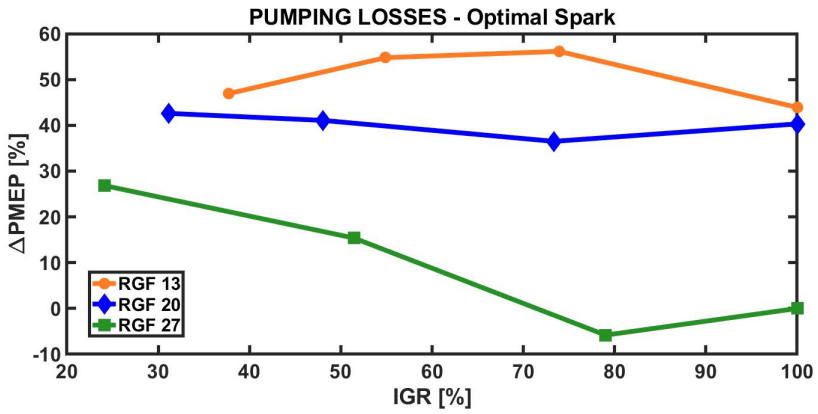

Figure 12: Pumping losses with respect to IGR for Optimal Spark tests.

In the same way as pumping losses, Figure 13 shows the brake specific fuel consumption variation in percentage with respect to the maximum IGR concentration of the 27% RGF level. The BSFC results show the same trend as pumping losses with respect to the RGF level, so a fuel economy improvement is achieved with higher total residuals. For 13 and 20% levels, the trend is to obtain a better fuel consumption with higher EGR rates probably due to reduced heat transfer losses. However, the reduced pumping losses achieved with increased IGR on the 27% level compensate the heat transfer losses, making the BSFC very flat with respect to IGR.

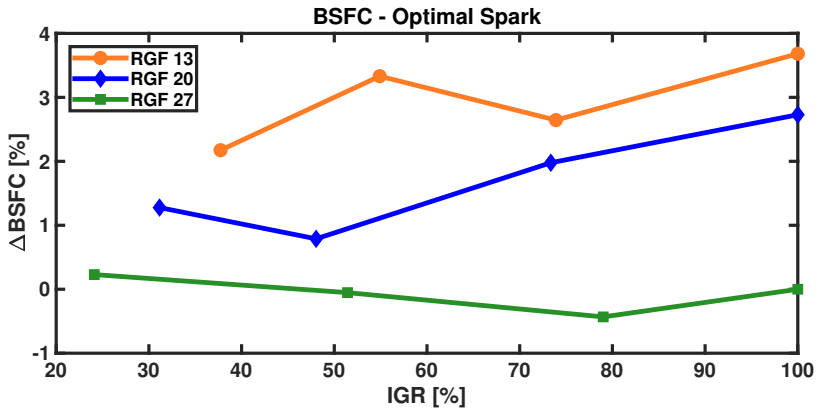

Figure 13: Brake specific fuel consumption with respect to IGR for Optimal Spark tests.

5.3. Gaseous emissions

In terms of emissions, Figure 14 shows a clear trend to reduce THC concentration with higher internal residuals due to two effects. In gasoline direct-injection engines, two of the main sources for these emissions are [42]:

- Flame extinction produced when reaching a crevice volume, including mainly the piston top-land section, but also others like the valve seats, cylinder head gaskets or the spark plug.
- Quenching of the flame when reaching a cold wall in the cylinder head, liner or piston surfaces.

Both aspects are controlled by heat transfer phenomena between the flame and the combustion chamber walls, and tend to be more significant as the laminar flame speed is lower [43]. Therefore, from the previous analysis it could be expected that HC emissions should be lower as the IGR would increase, with a higher sensitivity as the total RGF increases. This can actually be confirmed looking at Figure 14. However, it is interesting to note that the results for 13 and 20% RGF value are practically overlapped, despite some increase would have been expected for the 20% RGF condition attending to the combustion timing trends shown in Figure 9 and Figure 10, both of which indicate a decrease of

laminar flame speed with the total amount of residuals. The reason for this unexpected behavior may be linked to differences in the combustion chamber walls temperature.

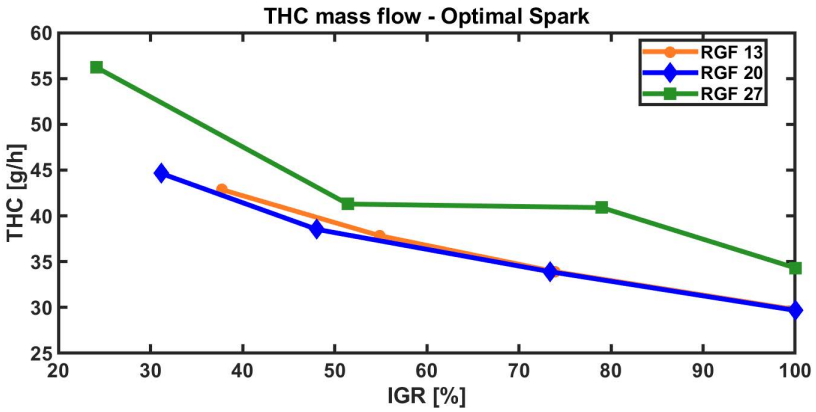

Figure 14: THC mass flow with respect to IGR for Optimal Spark tests.

Figure 15 shows the NOx concentration in the exhaust, in this case as a function of the calculated maximum temperature inside the cylinder during combustion, which is known to be the main driver for NOx. As expected, the temperature reduction obtained when combining higher RGF and cooled EGR concentrations, together with the lower oxygen concentration, is translated into a reduction in NOx formation as explained by the Zeldovich mechanism [44, 22].

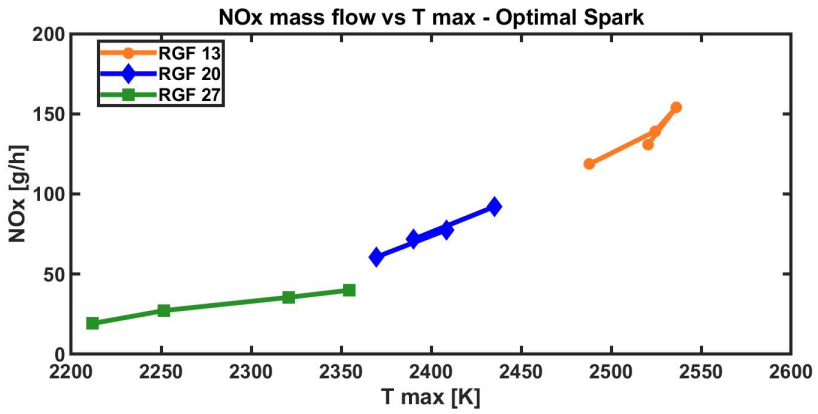

Figure 15: NOx mass flow with respect to peak combustion temperature for Optimal Spark tests.

Finally, CO formation depends highly on the CO to CO_2 reaction at the end of combustion. The reduction in the oxygen content inside the cylinder, which is more pronounced as RGF grows, should tilt the thermal equilibrium of the CO_2 dissociation reaction towards a higher CO production. However, the lower combustion temperature with higher RGF is translated into a reduced dissociation of CO_2, so in general lower CO is achieved as the RGF increases. Once the RGF level is fixed, the CO concentration tends in general to be reduced with IGR due to differences in the chemical kinetics of the dissociation reaction Figure 16.

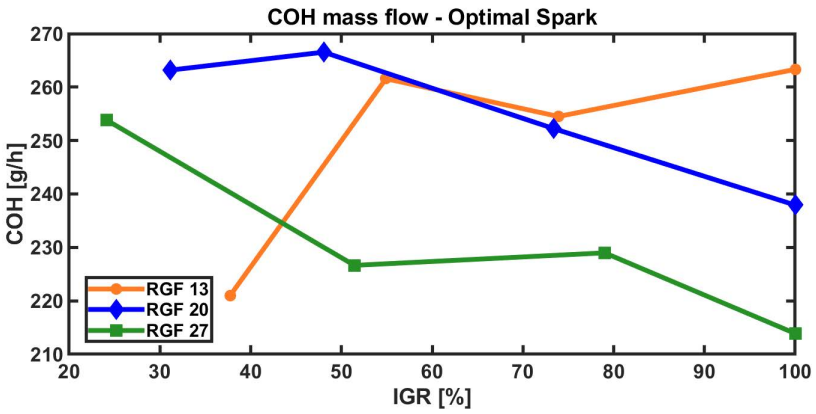

Figure 16: CO mass flow with respect to IGR for Optimal Spark tests.

For the operation with only IGR, NOx emissions are reduced along with CO, while HC emissions are slightly increased. Similar results were obtained in [4] with the exception of CO, which is very dependent on the CO_2 dissociation. Malaquias et al. [7] also reported a NOx and CO reduction of around 40 and 30% respectively, whereas HC is increased in most conditions.

6. Conclusions

In the current work, an investigation of the interaction between variable valve timing and cooled low-pressure exhaust gas recirculation systems as means to control the total residual gas fraction inside the cylinder is attempted from combustion perspective. While the variable valve timing controls the trapping ratio and therefore the amount of internal residuals remaining at the cylinder, the low-pressure EGR circuit allows to introduce higher amount of residuals without affecting significantly the engine breathing. Internal residuals and cooled EGR are characterized by different temperature and composition, since EGR is extracted after passing through the TWC, the study focuses on developing a methodology to decouple these two effects.

For this purpose, a first part of the investigation focuses on the analysis of specific tests aimed at reaching different total residuals levels with different

combinations of internal residuals and cooled EGR. This is achieved for two different testing strategies: a constant spark activation timing, so that geometric and flow characteristics are as close as possible for every EGR-IGR combination, and an adapted spark timing to reach the same in-cylinder temperature, so that the temperature effect can be better identified. The amount of internal residuals as well as the in-cylinder temperature are estimated using a previously developed and calibrated one-dimensional engine model. The following conclusions can be extracted from this part of the study:

- In general, both the induction time (defined as the lapse between the spark and the 10% of the total heat released) and the overall combustion duration (in terms of the time from 10 to 90 % of the heat released) tend to increase with the total RGF value, and decrease for higher shares of IGR.
- Once the temperature effect is decoupled, the decreasing trend with IGR is maintained for the highest values of RGF, while it disappears when the total amount of residuals is low.
- Temperature effect on the combustion timings can be directly linked to the impact of this parameter on the laminar flame speed according to existing correlations in the literature.
- Once the temperature and composition effects are properly accounted for, the total combustion duration can be reasonably predicted using the induction time and the spark timing as input parameters.

As a final step, the spark timing is optimized for each IGR-EGR combination to extract the following conclusions from energy balance and emissions perspective:

- The gross indicated efficiency shows a trend to increase with the total RGF level, while the sensitivity to the specific share of IGR is small, showing in general a benefit for cooled EGR. This is due to the fact that

shorter combustion timings for higher IGR are compensated by higher heat transfer and exhaust enthalpy losses.

- Pumping losses tend to be lower for higher combinations of RGF and IGR, partially compensating the better indicated efficiency reached for cooled EGR operation.

- Unburned hydrocarbons emissions are directly linked to laminar flame speed phenomena as a consequence of flame quenching effects both around crevice volumes and the main combustion chamber walls, being deteriorated for higher RGF while reduced as IGR increase.

- Nitrogen oxides emissions increase with lower RGF and higher IGR levels, as a consequence of their effects in the maximum combustion temperature. This parameter also shows a significant impact on CO, with a general trend to be reduced for higher RGF levels, while kinetic effects control the lower differences seen for the same RGF level.

7. Limitations and future works

The methodology described in the current work has helped to confirm that the individual effects of in-cylinder temperature and composition need to be considered when mixing external EGR and internal residuals. Additionally, the results from the constant temperature and the experimental correlations developed provide a first approximation at the quantification of each effect from combustion timings perspective. However, the methodology has some uncertainties and limitations that would need to be further assessed in future works:

- The estimation of the internal residuals is made through 1D engine simulations, due to the difficulty to have a direct measurement of this parameter on a multi-cylinder engine platform. Despite there is and indirect validation on the comparison with the air mass flow and the instantaneous pressure traces, shown in section 3.3, the lack of direct data for the internal residuals by itself an uncertainty in the methodology proposed. In

this sense, a similar work performed on a single-cylinder engine test bench, were it would be possible to have the internal residual measurement by the use of a tracer combined with skip fire operation, could be useful to further analyze this aspect.

- Apart from the mentioned effects from residuals temperature and composition, varying the VVT settings may result in variations in the tumble motion, affecting the turbulence field in the cylinder and therefore affecting overall combustion performance. Extending this work to different flow patterns would help to provide further insights about the interaction between al the phenomena involved.

- Current results show that there is some composition effect when comparing internal residuals (composed of uncatalyzed exhaust gases) and external EGR (mainly composed of nitrogen, CO_2 and water vapor). However, the specific contribution of each species is not evaluated. Since the exhaust gas composition would vary depending on the combustion characteristics, the results may be affected by calibration strategies and especially by the specifics of the combustion system layout. A detailed chemical kinetic study, starting from the selection of the mechanism for the fuel used without considering the residual effects, and then extending it to the operation with internal and external residuals considering their composition, is proposed.

- Related to the previous point, an extension of the methodology to fuels with different composition (particularly different H/C ratio) is proposed to widen the range of variation of the exhaust gas composition.

Acknowledgements

This research has been partially supported by the Ministry of Science and Innovation from the Government of Spain through project PID2020-114289RB-

I00. The authors would like to thank Mr. Vicente Esteve Ferrer for his collaboration during the experimental campaing and testing activities.

Greek symbols

α	Temperature exponent for laminar flame speed
β	Pressure exponent for laminar flame speed
τ	Time
ϕ	Equivalence ratio

Subscripts

0	Relative to standard conditions
ind	Relative to induction time
L	Relative to laminar
Spark	Relative to spark event
u	Relative to unburned zone

Abbreviations

a, b, c, d	correlation coefficients
BMEP	Break mean effective pressure
BSFC	Brake specific fuel consumption
bTDC	Before top dead center
CAD	Crank angle degree
CAX	Crank angle degree refered to X% of heat released
CI	Compression ignition
CO	Carbon monoxide
CO_2	Carbon dioxide
COV	Coefficient of variation
DoE	Design of experiments
ECU	Electronic control unit
EGR	Exhaust gas recirculation
EXH	Exhaust losses

GPF	Gasoline particle filter
HC	Unburnt hydrocarbon
HP-EGR	High-pressure exhaust gas recirculation
HT	In-cylinder heat transfer losses
IGR	Internal gas residual
IMEP	Indicated mean effective pressure
IND	Indicated efficiency
ISFC	Indicated specific fuel consumption
IVC	Intake valve closing
LP-EGR	Low-Pressure exhaust gas recirculation
MAPO	Maximum Amplitude of Pressure Oscillation
MFM	Mass flow meter
NEDC	New european driving cycle
NO_x	Nitrogen oxides
p	Pressure
PN	Particle Number
RGF	Residual gas fraction
rpm	Revolutions per minute
S	Flame speed
SI	Spark ignition
T	Temperature
TDC	Top dead center
THC	Total hydrocarbons
TOC	Time of combustion
TWC	Three-way catalyst
VGT	Variable geometry turbine
VVT	Variable valve timing
WCAC	Water charge air cooler

Appendix A: Main sensors and Horiba characteristics.

Table 9: Main sensors characteristics.

Magnitude	**Linearity**	**Range**
In-cylinder pressure	$\pm 0.3\%$	0 - 200 bar
Instantaneous pressure	$\leq \pm 0.2\%$	0 - 5 bar
Mean pressure	$\leq \pm 0.2\%$	0 - 5 bar
Charge amplifier	$< \pm 0.3\%$	2 - $2.2{\cdot}10^6$ pC
Mean temperature	$\pm 0.35\%$	270 - 1260°C
Air mass flow	$\pm 0.25\%$	0 - 1400 kg/h
Fuel mass flow	$\pm 0.12\%$	0 - 150 kg/h
Turbocharger speed	$\pm 0.2\%$	$2{\cdot}10^2$ -$4{\cdot}10^5$ rpm
Torquemeter	$\pm 0.1\%$	0 - 10 kN·m
Optical enconder	$\pm 0.006\%$	$2.5{\cdot}10^{-2}$ - $2.8{\cdot}10^4$ rpm

Table 10: Horiba MEXA-ONE characteristics.

Species	**Linearity**	**Range**
CO(L)	$< \pm$ 1%	0-3000 ppm
CO(H)	$< \pm$ 1%	0-10 vol%
CO_2	$< \pm$ 1%	0-20 vol%
THC	$< \pm$ 1%	0-25 K ppmC
$NMHC$, CH_4	$< \pm$ 1%	0-25 K ppmC
NO, NO_2, NO_x	$< \pm$ 1%	0-5000 ppm
O_2	$< \pm$ 1%	0-25 vol%

Appendix B: Empirical correlations

The effects of different compositions can be better assessed by developing empirical correlations based on the results achieved including individual terms

for internal and external residuals for the prediction of the combustion characteristic times. In this sense, the magnitude of the coefficients found in such correlations can provide an estimation of the relative impact of both parameters in combustion development. Additionally, fluid-dynamic engine models such as the one used for the estimation of the in-cylinder temperature and internal residuals along this paper, rely on empirical correlations for the prediction of the combustion profile, since they do not include a predictive combustion model. Therefore, the development of a proper correlation including the individual effects of internal and external residuals is necessary to enhance the predictive capability of such models.

In this sense, the following expression is proposed for the induction time prediction:

$$\tau_{ind} \quad [CAD] = (a \cdot RGF^{b} \cdot IGR^{c} \cdot \tau_{Spark}^{d}) \left(\frac{T_{Spark}}{T_0}\right)^{-1.67} \left(\frac{p_{Spark}}{p_0}\right)^{0.278} \tag{3}$$

where t_{ind} is the induction time defined as the difference between spark activation and CA10 in crank angle degrees, t_{Spark} refers to the spark activation timing in CAD bTDC, T_{Spark} and p_{Spark} are the temperature and pressure conditions estimated from the GT-Power model at that spark timing, and a, b, c, d are the coefficients adjusted during the correlation. Note that the exponents for temperature and pressure conditions at the spark timing are the same ones provided by Amirante et al. [39] for gasoline fuel, as introduced during the discussion of Equation 2, but with the opposite sign since a higher laminar flame speed value would result in a shorter induction time. The spark activation timing is included in the correlation in order to account for the different turbulent kinetic energy conditions around the spark area as a function of the piston position.

Two correlations have been tried, including or not the individual effect of the IGR level, as a way to evaluate the relative importance of accounting for the composition effect. The coefficients obtained for both correlations as well as their statistical significance in terms of R-squared parameter are summarized

Table 11: Results of the empirical correlations for the induction time.

Parameter	**w/ IGR**		**w/o IGR**	
	Value	**Interval 95%**	**Value**	**Interval 95%**
a	1.98	[1.5, 2.4]	0.94	[0.6, 1.3]
b	0.12	[0.08, 0.16]	0.23	[0.09, 0.37]
c	-0.15	[-0.19, -0.11]	-	-
d	0.3	[0.24, 0.36]	0.23	[0.13,0.33]
R^2	92.15		77.3	
$R^2 - adj$	90.97		75.2	

in Table 11. As it can be seen, the capability of the correlation to reproduce the model data is significantly impaired when the internal residuals amount is not considered, achieving a decrease around 15% in terms of R-squared. The output of both correlations is depicted in an observed vs. predicted graph in Figure 17. For the first correlation considering the IGR effect, almost all predicted values fall into a ± 1 CAD band, and the average deviation is 0.6 CAD. Instead, the second correlation including only RGF term shows a significantly higher deviation with respect to the experiments in general, with an average and maximum deviations of 1.1 and 3 CAD, respectively.

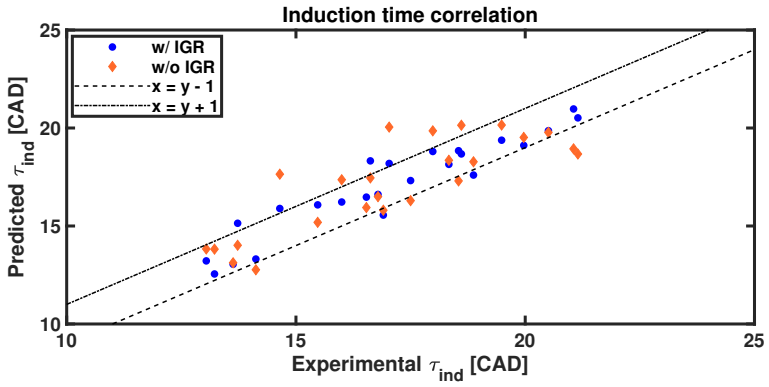

Figure 17: Experimental vs. predicted induction time for correlations with and without considering IGR.

Regarding the overall combustion duration (TOC), the following correlation has been tried:

$$TOC \quad [CAD] = a \cdot \tau_{ind}^{b} \cdot \tau_{Spark}^{c} \tag{4}$$

In this case, the induction time intends to include all laminar flame speed aspects (including both temperature and composition) and the spark timing tries to consider again the turbulence effect. However, it has to be acknowledged that the combustion duration is known to be more significantly affected by the turbulence field inside the cylinder, so a more detailed consideration of turbulence phenomena should be considered for future works. However, the results from this simple evaluation can be seen in Table 12 and Figure 18. As expected, the correlation achieved is less predictive compared to the one already analyzed for the induction time, achieving around 6% lower R-squared and a higher deviation in general with respect to the experimental data. Nevertheless, the mean deviation of 0.7 CAD and the maximum deviation of 1.66 CAD achieved can be seen as an adequate result for the estimation of the combustion duration in one-dimensional engine simulation environment.

Table 12: Results of the empirical correlations for the combustion duration.

Parameter	Value	Interval 95%
a	0.63	[0.46, 0.80]
b	1.48	[1.22, 1.73]
c	-0.35	[-0.44, -0.26]
R^2	86.85	
$R^2 - adj$	85.60	

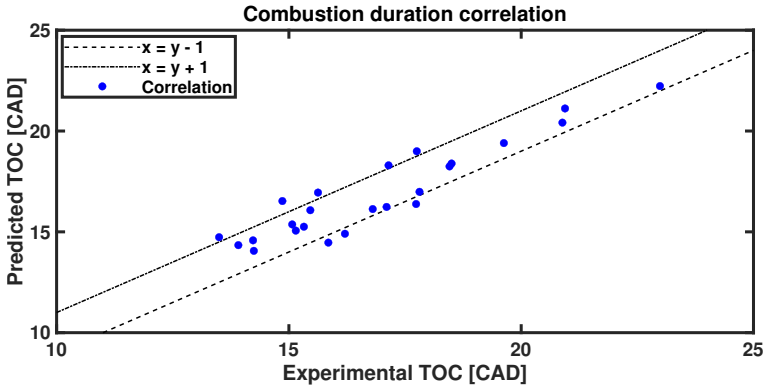

Figure 18: Experimental vs. predicted combustion duration.

References

[1] G. Shu, J. Pan, H. Wei, Analysis of onset and severity of knock in SI engine based on in-cylinder pressure oscillations, Applied Thermal Engineering 51 (1-2) (2013) 1297–1306. doi:10.1016/j.applthermaleng.2012.11.039.
URL http://dx.doi.org/10.1016/j.applthermaleng.2012.11.039

[2] A. Joshi, Review of Vehicle Engine Efficiency and Emissions, SAE Technical Papers 2 (2021) (2021) 2479–2507. doi:10.4271/2021-01-0575.

[3] G. Fontana, E. Galloni, Variable valve timing for fuel economy improvement in a small spark-ignition engine, Applied Energy 86 (2009) 96–105. doi:10.1016/j.apenergy.2008.04.009.

[4] S. Szwaja, E. Ansari, S. Rao, M. Szwaja, K. Grab-Rogalinski, J. D. Naber, M. Pyrc, Influence of exhaust residuals on combustion phases, exhaust toxic emission and fuel consumption from a natural gas fueled spark-ignition engine, Energy Conversion and Management 165 (December 2017) (2018) 440–446. doi:10.1016/j.enconman.2018.03.075.

[5] T. D. M. Lanzanova, M. Dalla Nora, M. E. S. Martins, P. R. M. Machado, V. B. Pedrozo, H. Zhao, The effects of residual gas trapping on part load performance and emissions of a spark ignition direct injection engine fuelled with wet ethanol, Applied Energy 253 (January) (2019) 113508. doi:10.1016/j.apenergy.2019.113508.
URL https://doi.org/10.1016/j.apenergy.2019.113508

[6] N. X. Khoa, Y. Quach Nhu, O. Lim, Estimation of parameters affected in internal exhaust residual gases recirculation and the influence of exhaust residual gas on performance and emission of a spark ignition engine, Applied Energy 278 (June) (2020) 115699. doi:10.1016/j.apenergy.2020.115699.
URL https://doi.org/10.1016/j.apenergy.2020.115699

[7] A. C. T. Malaquias, N. A. D. Netto, R. B. R. da Costa, J. G. C. Baêta, Combined effects of internal exhaust gas recirculation and tumble motion generation in a flex-fuel direct injection engine, Energy Conversion and Management 217 (March) (2020) 113007. doi:10.1016/j.enconman.2020.113007.
URL https://doi.org/10.1016/j.enconman.2020.113007

[8] T. Li, D. Wu, M. Xu, Thermodynamic analysis of EGR effects on the first and second law efficiencies of a boosted spark-ignited direct-injection

gasoline engine, Energy Conversion and Management 70 (x) (2013) 130–138. doi:10.1016/j.enconman.2013.03.001.

[9] L. Marchitto, C. Tornatore, G. Valentino, L. Teodosio, Impact of Cooled EGR on Performance and Emissions of a Turbocharged Spark-Ignition Engine under Low-Full Load Conditions, SAE Technical Paper (2019). doi:10.4271/2019-24-0021.

[10] A. Cairns, N. Fraser, H. Blaxill, Pre Versus Post Compressor Supply of Cooled EGR for Full Load Fuel Economy in Turbocharged Gasoline Engines, SAE Technical Paper 2008-01-0425 (2008).

[11] J. P. Szybist, S. W. Wagnon, D. Splitter, W. J. Pitz, M. Mehl, The Reduced Effectiveness of EGR to Mitigate Knock at High Loads in Boosted SI Engines, SAE Technical Paper 2017-24-0061 (2017). doi:10.4271/2017-24-0061.

[12] D. Parsons, S. Orchard, N. Evans, U. Ozturk, R. Burke, C. Brace, A comparative study into the effects of pre and post catalyst exhaust gas recirculation on the onset of knock, International Journal of Engine Research (2020). doi:10.1177/1468087420962294.

[13] F. Bozza, V. De Bellis, L. Teodosio, Potentials of cooled EGR and water injection for knock resistance and fuel consumption improvements of gasoline engines, Applied Energy 169 (2016) 112–125. doi:10.1016/j.apenergy.2016.01.129.
URL http://dx.doi.org/10.1016/j.apenergy.2016.01.129

[14] A. H. Kakaee, M. H. Shojaeefard, J. Zareei, Sensitivity and effect of ignition timing on the performance of a spark ignition engine: An experimental and modeling study, Journal of Combustion 2011 (2011). doi:10.1155/2011/678719.

[15] J. Su, M. Xu, T. Li, Y. Gao, J. Wang, Combined effects of cooled EGR and a higher geometric compression ratio on thermal effi-

ciency improvement of a downsized boosted spark-ignition direct-injection engine, Energy Conversion and Management 78 (2014) 65–73. doi:10.1016/j.enconman.2013.10.041.
URL http://www.sciencedirect.com/science/article/pii/S0196890413006766

[16] S. Zhang, Y. Li, S. Wang, H. Zeng, J. Liu, X. Duan, H. Dong, Experimental and numerical study the effect of EGR strategies on in-cylinder flow, combustion and emissions characteristics in a heavy-duty higher CR lean-burn NGSI engine coupled with detail combustion mechanism, Fuel 276 (February) (2020) 118082. doi:10.1016/j.fuel.2020.118082.
URL https://doi.org/10.1016/j.fuel.2020.118082

[17] X. Yu, Z. Zhao, Y. Huang, W. Shi, Z. Guo, Z. Li, Y. Du, Z. Jin, D. Li, T. Wang, Y. Li, Experimental study on the effects of EGR on combustion and emission of an SI engine with gasoline port injection plus ethanol direct injection, Fuel 305 (August) (2021) 121421. doi:10.1016/j.fuel.2021.121421.
URL https://doi.org/10.1016/j.fuel.2021.121421

[18] H. Oh, J. Lee, S. Woo, H. Park, Effect of synergistic engine technologies for 48 V mild hybrid electric vehicles, Energy Conversion and Management 244 (May) (2021) 114515. doi:10.1016/j.enconman.2021.114515.
URL https://doi.org/10.1016/j.enconman.2021.114515

[19] C. Gong, X. Si, F. Liu, Combustion and emissions behaviors of a stoichiometric GDI engine with simulated EGR (CO2) at low load and different spark timings, Fuel 295 (December 2020) (2021) 120614. doi:10.1016/j.fuel.2021.120614.
URL https://doi.org/10.1016/j.fuel.2021.120614

[20] E. Galloni, G. Fontana, R. Palmaccio, Effects of exhaust gas recycle in a downsized gasoline engine, Applied Energy 105 (2013) 99–107. doi:

10.1016/j.apenergy.2012.12.046.
URL http://dx.doi.org/10.1016/j.apenergy.2012.12.046

[21] C. Yu, Z. Zhao, L. Wang, H. Cui, F. Zhang, The effect of cooled EGR on combustion and load extension in a kerosene spark-ignition engine, Fuel 280 (March) (2020) 118681. doi:10.1016/j.fuel.2020.118681.
URL https://doi.org/10.1016/j.fuel.2020.118681

[22] F. Xie, X. Li, Y. Su, W. Hong, B. Jiang, L. Han, Influence of air and EGR dilutions on improving performance of a high compression ratio spark-ignition engine fueled with methanol at light load, Applied Thermal Engineering 94 (2016) 559–567. doi:10.1016/j.applthermaleng.2015.10.046.
URL http://dx.doi.org/10.1016/j.applthermaleng.2015.10.046

[23] J. M. Luján, H. Climent, R. Novella, M. E. Rivas-Perea, Influence of a low pressure EGR loop on a gasoline turbocharged direct injection engine, Applied Thermal Engineering 89 (2015) 432–443. doi:10.1016/j.applthermaleng.2015.06.039.

[24] A. Reihani, J. Hoard, S. Klinkert, C. K. Kuan, D. Styles, G. McConville, Experimental response surface study of the effects of low-pressure exhaust gas recirculation mixing on turbocharger compressor performance, Applied Energy 261 (December 2019) (2020) 114349. doi:10.1016/j.apenergy.2019.114349.
URL https://doi.org/10.1016/j.apenergy.2019.114349

[25] V. Bermúdez, J. M. Lujan, H. Climent, D. Campos, Assessment of pollutants emission and aftertreatment efficiency in a GTDi engine including cooled LP-EGR system under different steady-state operating conditions, Applied Energy 158 (2015) 459–473. doi:10.1016/j.apenergy.2015.08.071.

[26] T. Franken, F. Mauss, L. Seidel, M. S. Gern, M. Kauf, A. Matrisciano,

A. C. Kulzer, Gasoline engine performance simulation of water injection and low-pressure exhaust gas recirculation using tabulated chemistry, International Journal of Engine Research (in press) (2020). doi:10.1177/1468087420933124.
URL https://doi.org/10.1177/1468087420933124

[27] T. Lattimore, C. Wang, H. Xu, M. L. Wyszynski, S. Shuai, Investigation of EGR Effect on Combustion and PM Emissions in a DISI Engine, Applied Energy 161 (x) (2016) 256–267. doi:10.1016/j.apenergy.2015.09.080.
URL http://dx.doi.org/10.1016/j.apenergy.2015.09.080

[28] S. Fontanesi, M. D. Pecchia, V. Pessina, S. Sparacino, S. D. Iorio, Quantitative investigation on the impact of injection timing on soot formation in a GDI engine with a customized sectional method, International Journal of Engine Research (in press) (2021). doi:10.1177/1468087421993955.

[29] L. Zhao, X. Su, X. Wang, Comparative study of exhaust gas recirculation (EGR) and hydrogen-enriched EGR employed in a SI engine fueled by biobutanol-gasoline, Fuel 268 (October 2019) (2020) 117194. doi:10.1016/j.fuel.2020.117194.
URL https://doi.org/10.1016/j.fuel.2020.117194

[30] B. Gainey, Z. Yan, S. Moser, B. Lawler, Lean flammability limit of high-dilution spark ignition with ethanol, propanol, and butanol, International Journal of Engine Research (2021) 1–11doi:10.1177/1468087421993256.

[31] J. Galindo, H. Climent, J. De la Morena, D. González-Domínguez, S. Guilain, T. Besançon, Experimental and modeling analysis on the optimization of combined VVT and EGR strategies in turbocharged direct-injection gasoline engines with VNT, Proceedings of the Institution of Mechanical Engineering. Part D-Journal of Automobile Engineering (2021 (in press)).

[32] V. De Bellis, E. Severi, S. Fontanesi, F. Bozza, Hierarchical 1D/3D approach for the development of a turbulent combustion model applied to a

VVA turbocharged engine. Part II: Combustion model, Energy Procedia 45 (2014) 1027–1036. doi:10.1016/j.egypro.2014.01.108.
URL http://dx.doi.org/10.1016/j.egypro.2014.01.088

[33] B. Pla, J. De La Morena, P. Bares, I. Jiménez, Knock Analysis in the Crank Angle Domain for Low-Knocking Cycles Detection, SAE Technical Papers 2020-April (April) (2020) 1–11. doi:10.4271/2020-01-0549.

[34] P. Piqueras, J. De la Morena, E. J. Sanchis, R. Pitarch, Impact of Exhaust Gas Recirculation on Gaseous Emissions of Turbocharged Spark-Ignition Engines, Applied Sciences 10 (7634) (2020) 1–17. doi:10.3390/app10217634.

[35] Z. Zhang, T. Wang, M. Jia, Q. Wei, X. Meng, G. Shu, Combustion and particle number emissions of a direct injection spark ignition engine operating on ethanol/gasoline and n-butanol/gasoline blends with exhaust gas recirculation, Fuel 130 (2014) 177–188. doi:10.1016/j.fuel.2014.04.052.
URL http://dx.doi.org/10.1016/j.fuel.2014.04.052

[36] J. Serrano, H. Climent, R. Navarro, D. González-Domínguez, Methodology to Standardize and Improve the Calibration Process of a 1D Model of a GTDI Engine, SAE Technical Papers 2020-April (April) (2020) 1–13. doi:10.4271/2020-01-1008.

[37] F. Payri, J. J. López, J. Martín, R. Carreño, Improvement and application of a methodology to perform the global energy balance in internal combustion engines. part 1: Global energy balance tool development and calibration, Energy 152 (2018) 666–681. doi:https://doi.org/10.1016/j.energy.2018.03.118.
URL https://www.sciencedirect.com/science/article/pii/S0360544218305279

[38] G. A. Lavoie, E. Ortiz-soto, A. Babajimopoulos, J. B. Martz, D. N. Assanis, Thermodynamic sweet spot for high- efficiency, dilute, boosted gasoline

engines, International Journal of Engine Research 14 (3) (2012) 260–278. doi:10.1177/1468087412455372.

[39] R. Amirante, E. Distaso, P. Tamburrano, R. D. Reitz, Laminar flame speed correlations for methane, ethane, propane and their mixtures, and natural gas and gasoline for spark-ignition engine simulations, International Journal of Engine Research 18 (9) (2017) 951–970. doi:10.1177/1468087417720018.

[40] R. O. Grover, Jr., D. Cleary, Correlating Measured Combustion Performance with CFD Predicted In-Cylinder Flows for a Spark-Ignition Direct-Injection (SIDI) Engine with Enhanced Charge Motion (2013). doi:10.4271/2013-01-1090.
URL http://papers.sae.org/2013-01-1090/

[41] A. Nishiyama, M. K. Le, T. Furui, Y. Ikeda, The Relationship between In-Cylinder Flow-Field near Spark Plug Areas, the Spark Behavior, and the Combustion Performance inside an Optical S.I. Engine, Applied Sciences 9 (8) (2019) 1545. doi:10.3390/app9081545.
URL https://www.mdpi.com/2076-3417/9/8/1545

[42] M. Dorsch, J. Neumann, C. Hasse, Application of a Phenomenological Model for the Engine-Out Emissions of Unburned Hydrocarbons in Driving Cycles, Journal of Energy Resources Technology 138 (2) (2016) 22201. doi:10.1115/1.4031674.

[43] S. Esposito, L. Diekhoff, S. Pischinger, Prediction of gaseous pollutant emissions from a spark-ignition direct-injection engine with gas-exchange simulation, in: THIESEL 2020 Conference on Thermo- and Fluid Dynamic Processes in Direct Injection Engines, 2020, pp. 1–20.

[44] H. Wei, T. Zhu, G. Shu, L. Tan, Y. Wang, Gasoline engine exhaust gas recirculation – A review, Applied Energy 99 (2012) 534–544. doi:10.1016/j.apenergy.2012.05.011.

URL http://linkinghub.elsevier.com/retrieve/pii/S0306261912003595